Eleventh International Conference on CFD in the Minerals and Process Industries
CSIRO, Melbourne, Australia
7-9 December 2015

HIGH RESOLUTION SIMULATION REVEALING $RA^{1/4}$ SCALING REGIME FOR NUSSELT NUMBER IN HORIZONTAL CONVECTION

Tzekih TSAI[1]*, **Martin P. KING**[2], **Gregory J. SHEARD**[1]

[1]The Sheard Lab, Department of Mechanical and Aerospace Engineering, Monash University, VIC 3800, Australia

[2]Uni Research, and Bjerknes Centre for Climate Research, NO 5007, Bergen, Norway

* E-mail: tzekih.tsai@monash.edu

ABSTRACT

A non-uniform thermal forcing imposed along a horizontal boundary gives rise to horizontal convective flow, which finds application as a simple model to study ocean circulation, the Earth's mantle convection and industrial processes. The strength of thermal forcing is characterised by the Rayleigh number. At high Rayleigh numbers, horizontal convection is convectively dominant, featuring thin thermal and velocity boundary layers adjacent to the forcing boundary. At sufficiently high Rayleigh numbers, horizontal convection flow has been observed to become unsteady. The scaling of Nusselt number, quantifying heat transport, and the Rayleigh number quantifying thermal forcing, yields a 1/5-power scaling which is well understood at low Rayleigh number. In this study, a high-order spectral element solver is used to study horizontal convection at high Rayleigh number within a rectangular enclosure with buoyancy forcing imposed along a horizontal forcing boundary. These high-resolution simulations provide insight into the dynamics of horizontal convection at high Rayleigh number to reveal the existence of a 1/4-power scaling. This 1/4-regime is generated by the horizontal convection of cooler fluid over the hot end of the forcing boundary, spontaneous plume eruptions upstream of the enclosure end-wall carry heat directly into the interior overturning flow. This violates Rossby's balance between vertical thermal diffusion from the boundary into the adjacent boundary layer and the horizontal transport of heat within the boundary layer.

NOMENCLATURE

Latin Symbols

c_p	fluid specific heat capacity
F_T	heat flux per unit area
g	gravitational acceleration
$\hat{\mathbf{g}}$	unit vector in direction of gravity
H	height of enclosure
h	boundary layer thickness scale
h_u	kinematic boundary layer thickness scale
h_θ	thermal boundary layer thickness scale
L	width of enclosure
Nu	Nusselt number
p	pressure
Pr	Prandtl number
Ra	Rayleigh number
Ra_F	flux Rayleigh number
Sh	Sherwood number
t	time
$\mathbf{u}$	velocity vector
u	x component velocity
v	y component velocity
x	Cartesian horizontal coordinate
y	Cartesian vertical coordinate

Greek Symbols

α	volumetric expansion coefficient
κ	fluid thermal diffusivity
μ	fluid kinematic viscosity
ρ	fluid density
θ	temperature
$\delta\theta$	horizontal temperature difference along base

Sub/superscripts

0	reference value

INTRODUCTION

Horizontal convection describes convection flow driven in an enclosure by non-uniform heating imposed across a horizontal boundary (Hughes and Griffiths, 2008), and serves as a model for global ocean currents (Stommel, 1962; Huang, 1999; Wunsch and Ferrari, 2004). These flows are characterised by a Rayleigh number *Ra* representing the strength of buoyancy over dissipative effects, and a Prandtl number *Pr* representing the ratio of molecular to thermal dissipation in the fluid. Overturning flow exists at all Rayleigh numbers, while higher Rayleigh numbers invoke a convective regime characterised by thin thermal and kinematic boundary layers adjacent to the forcing boundary that scale inversely with Nusselt number *Nu* (Mullarney *et al.*, 2004) characterising the horizontal heat transport. This overturning flow acts similarly to the "wind of turbulence" in Rayleigh–Bénard convection, forging an important connection to Grossmann and Lohse's unifying theory of thermal convection (Grossmann and Lohse, 2000, 2001, 2002). The scaling of Nusselt number with Rayleigh number is critical to our understanding of the role of buoyancy destabilisation in driving global ocean currents (Siggers *et al.*, 2004; Mullarney *et al.*, 2004; Hughes and Griffiths, 2008; Barkan *et al.*, 2013). In horizontal convection, Nusselt number is based on the net vertical heat flux over the thermal forcing bound-

ary.

Rossby (1965) developed scalings for forcing boundary layer quantities in thermal convection heated unevenly from below. Assuming a balance between vertical thermal diffusion into the thermal boundary layer from the base and horizontal transport of heat within the boundary layer leads to scaling of boundary layer thickness as $h \sim Ra^{-1/5}$ and Nusselt number as $Nu \sim Ra^{1/5}$.

Evidence supporting Rossby's scalings at Rayleigh numbers sufficient to invoke the convective regime is plentiful. Numerical and laboratory experiments by Mullarney *et al.* (2004) demonstrated a Nusselt number scaling against a thermal flux-based Rayleigh number $Nu \sim Ra_F^{1/6}$ equivalent to a $Ra^{1/5}$ scaling, while other numerical studies have directly demonstrated the $Nu \sim Ra^{1/5}$ scaling up to Rayleigh numbers $Ra = O(10^9)$ (Siggers *et al.*, 2004; Sheard and King, 2011) and $Ra = O(10^7)$ (Chiu-Webster *et al.*, 2008). Numerical simulations by Sheard and King (2011) and Ilıcak and Vallis (2012) each demonstrated a $Ra^{-1/5}$ scaling for forcing boundary layer thickness.

These flows were known to become unsteady beyond some Rayleigh number (Sheard and King, 2011) reported unsteady flow beyond $Ra = 6 \pm 2.5 \times 10^8$ while Ilıcak and Vallis (2012) observed unsteady flow for $Ra > 10^{10}$. The effect of unsteady flow on horizontal convection scalings was first recognised by Sheard and King (2011), where simulations across several enclosure height ratios demonstrated *Nu–Ra* scaling exponents exceeding $1/5$. Theoretical support for higher power-law exponents in the scaling for *Nu* is availed by the variational analysis of Siggers *et al.* (2004), which places an upper bound of $1/3$ on the scaling exponent.

An alternative explanation for the behaviour of horizontal convection was offered by Gayen *et al.* (2014) from three-dimensional numerical simulations conducted at $Pr = 5$ across Rayleigh numbers $5.86 \times 10^7 \leq Ra \leq 5.86 \times 10^{14}$ in an enclosure with height-to-width ratio $H/L = 0.16$. They observed Nusselt numbers exceeding the $Ra^{1/5}$ scaling regime beyond $Ra = O(10^8)$, before settling onto a second regime exhibiting $Ra^{1/5}$ scaling at elevated Nusselt numbers beyond $Ra = O(10^{12})$. An explanation for this recovered $Ra^{1/5}$ scaling at higher Rayleigh numbers is offered by a simple model based on a local vertical turbulent plume from a line source that maintains a stably stratified interior (Hughes *et al.*, 2007). Despite the different construction to Rossby's scaling argument, this model predicts the same $Nu \sim Ra_F^{1/6} \sim Ra^{1/5}$ scaling.

This study aims to resolve the apparent shift in the scaling exponent at high Rayleigh numbers (Sheard and King, 2011; Gayen *et al.*, 2014).

METHODOLOGY

The system (Figure 1) comprises a rectangular enclosure of width L and height H filled with an incompressible fluid with kinematic viscosity ν, thermal diffusivity κ, reference temperature θ_0 and reference density ρ_0. The enclosure aligns with a Cartesian coordinate system with x and y being the horizontal and vertical coordinates, respectively. The origin is at the bottom-left corner of the enclosure. Lengths, time (t), velocity vector ($\mathbf{u} = \langle u, v \rangle$), pressure ($p$) and temperature ($\theta$) are respectively scaled by L, L^2/κ, κ/L, $\rho_0 \kappa^2/L^2$ and $\delta\theta$ (the temperature differential imposed across the forcing boundary). All quantities are expressed in their dimensionless form hereafter, and p and θ are hereafter taken relative to their respective reference values. All boundaries are rigid and impermeable, satisfying the no-slip condition $\mathbf{u} = 0$. Adiabatic boundary conditions are imposed on side and top boundaries, while along the forcing boundary a linear temperature profile is imposed ranging from $\theta = 0$ at $(x,y) = (0,0)$ to $\theta = 1$ at $(x,y) = (1,0)$. A Boussinesq model for buoyancy is employed, whereby density changes ($\rho = 1 - \alpha\theta$) are assumed to be small and are therefore isolated to a buoyancy term in the momentum equation. The equations governing conservation of mass, momentum and energy are therefore

$$\nabla \cdot \mathbf{u} = 0, \tag{1}$$

$$\partial_t \mathbf{u} + (\mathbf{u} \cdot \nabla)\mathbf{u} = -\nabla p + Pr\nabla^2 \mathbf{u} - PrRa\,\hat{\mathbf{g}}\,\theta, \tag{2}$$

$$\partial_t \theta + (\mathbf{u} \cdot \nabla)\theta = \nabla^2 \theta, \tag{3}$$

where ∂_t represents partial differentiation with respect to time, and $\hat{\mathbf{g}}$ is a unit vector in the direction of gravity (here acting vertically downward). Equation (2) incorporates the Prandtl number $Pr = \nu/\kappa$ and the Rayleigh number $Ra = \alpha g\,\delta\theta L^3/\nu\kappa$.

Equations (1)-(3) are solved using a nodal spectral element method for spatial discretisation and a third-order operator-splitting scheme based on backwards-differentiation for time integration (Karniadakis *et al.*, 1991). The scheme achieves exponential convergence with increasing element polynomial order (Karniadakis and Sherwin, 2005), negligible diffusion error (Giraldo, 1998) and minimal dispersion error (Giannakouros and Karniadakis, 1994; Giraldo, 1998). It combines the flexibility of finite-element methods for localised mesh refinement with the superior convergence properties of spectral methods with increasing element order. Further details and validation of the code is supplied in (Sheard and King, 2011; Hussam *et al.*, 2014).

Simulations are performed in an enclosure with $H/L = 0.16$ matching published works (Mullarney *et al.*, 2004; Sheard and King, 2011; Gayen *et al.*, 2014): (Sheard and King, 2011) demonstrates H/L independence for $H/L \geq 0.16$ beyond $Ra = O(10^8)$. We consider only Prandtl number $Pr = 6.14$, representative of water, due to the motivating interest in

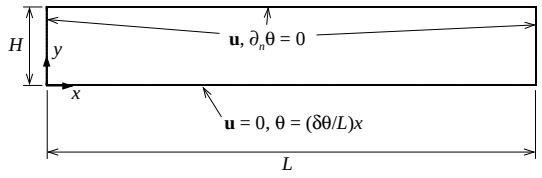

Figure 1: Schematic representation of the system under investigation. The enclosure has width L and height H, and boundary conditions on velocity ($\mathbf{u}$) and temperature (θ) are labelled, with ∂_n denoting the partial derivative with respect to an outward normal to the boundary.

global ocean circulation. The domain is discretized into a conforming grid of 3692 quadrilateral spectral elements with degree ranging from 6 at lower Ra up to 10 for $Ra = 3.2 \times 10^{13}$. Elements are concentrated towards the bottom forcing boundary and the hot end of the enclosure to capture the boundary layers, plume and any unstable flow structures. Simulations therefore contained between 711×131 6th-order interpolation points and 1279×235 10th-order interpolation points, an unparalleled resolution for direct simulation of horizontal convection over the computed Rayleigh number range $Ra \leq 3.2 \times 10^{13}$. All simulations are time-evolved to a statistically steady state before time-averaged Nu are calculated.

RESULTS

Direct horizontal convection solutions are obtained up to $Ra = 3.2 \times 10^{13}$. Unsteady flow in the form of a time-periodic equilibrium state first appears at $Ra = 5.5 \times 10^8$, refining earlier reported values $3.5 \times 10^8 < Ra < 8.5 \times 10^8$ (Sheard and King, 2011) and $Ra < 5.86 \times 10^8$ (Gayen *et al.*, 2014). Time-periodic flow quickly gives way to an irregular regime with increasing Rayleigh number beyond $Ra \approx 1.8 \times 10^9$.

The dependence of Nusselt number on Rayleigh number is shown in Figure 2. The convective regime establishes beyond $Ra = O(10^7)$ (labelled as regime I), adopting Rossby's $Ra^{1/5}$ scaling. The $Ra^{1/5}$ scaling holds through the time-periodic regime (II), but the onset of the irregular flow regime (III) brings an elevated scaling for Nusselt number going with $Ra^{0.24\pm0.01}$. Inspection of Figure 3 in (Sheard and King, 2011) reveals that their increased Nusselt number scaling beyond $Ra = O(10^9)$ in fact adopted a scaling exponent of 0.25, consistent with this regime. Hence rather than an approach of the scaling exponent towards the theoretical upper bound of $1/3$ (Siggers *et al.*, 2004), these results may represent the influence of a scaling regime with an exponent of $1/4$. This regime is robust, adhering close to $Ra^{1/4}$ for more than four decades in Rayleigh number.

A physical understanding of this $Ra^{1/4}$ regime is aided by consideration of the vertical thermal gradient, $\partial\theta/\partial y$, along the forcing boundary. Where Rossby's $Ra^{1/5}$ scaling holds, $\partial\theta/\partial y$ at different Rayleigh numbers should coincide when scaled by $Ra^{1/5}$. Figure 3 compares two cases: a borderline regime I/II case ($Ra = 5.5 \times 10^8$) exhibiting to the $Ra^{1/5}$ scaling in Figure 2, and a regime III case ($Ra = 1 \times 10^{11}$) exhibiting $Ra^{1/4}$ scaling. Along much of the forcing boundary, the normalised thermal gradients are coincident. Beyond $x \approx 0.94$, the higher-Ra case exhibits a significant increase in thermal gradient. This in turn increases Nusselt number beyond Rossby's $Ra^{1/5}$ scaling. The elevated thermal gradients are produced across the hottest part of the base where unsteady flow features manifest in the form of buoyant mushroom plumes ascending from the forcing boundary upstream of the end-wall (compare the instantaneous thermal fields in Figure 3).

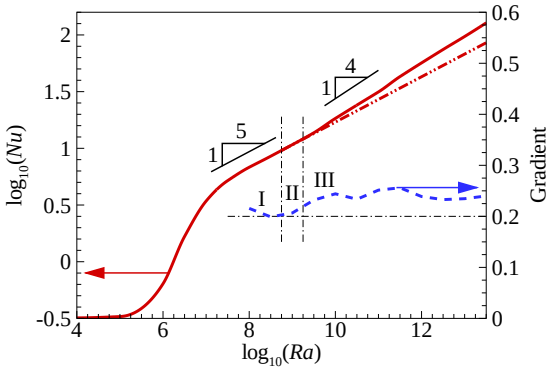

Figure 2: Plots of $\log_{10}(Nu)$ and its gradient against $\log_{10}(Ra)$. $1/5$ and $1/4$ gradient indicators are included for guidance, and labels I, II and III identify the respective steady-state, time periodic and plume eruption convection regimes. Regimes I and II follow Rossby's scaling (extrapolated along the dash-dot-dot line) described by $Nu = 0.171Ra^{1/5}$, while four decades of Rayleigh number through regime III consistently demonstrate a $Ra^{1/4}$ scaling adhering to $Nu = 0.59Ra^{1/4}$. The threshold between $1/5$ and $1/4$ regimes is $Ra \approx 1.8 \times 10^9$.

Why do these plumes increase the heat transport? Locally, the thermal boundary layer in stable horizontal convection is analogous to a forced-convection scenario: heat enters the boundary layer from the hot boundary via conduction, and is transported horizontally within the kinematic boundary layer established as part of the global overturning flow. At Prandtl numbers $Pr \gg 1$ such as in this study, the thermal boundary layer is nested within the kinematic boundary layer, so there is no heat transport across the boundary layer into the interior. This is instead facilitated by the vertical plume at the hot end-wall. In contrast, within the unsteady plume eruption region a natural-convection scenario is created: buoyancy supply to the fluid is sufficient to disrupt the horizontal transport within the boundary layer, and hot fluid is trans-

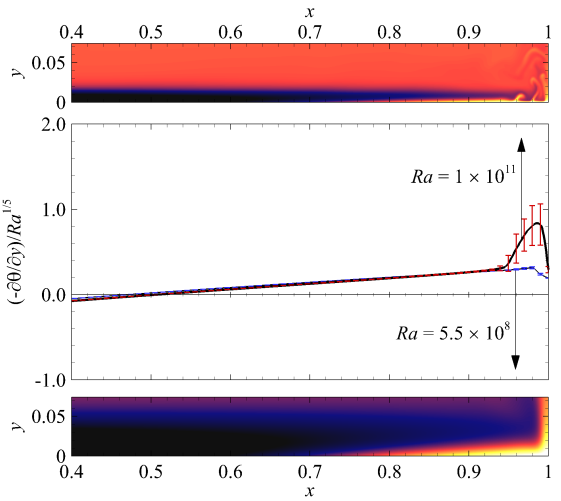

Figure 3: A plot of $-(\partial\theta/\partial y)/Ra^{1/5}$ against x over the hotter 60% of the forcing boundary. Rayleigh numbers $Ra = 5.5 \times 10^8$ and 1×10^{11} are shown. Solid lines show the time mean data, and error bars the standard deviation. Instantaneous temperature fields for the two Rayleigh numbers are included above and below the plot, respectively.

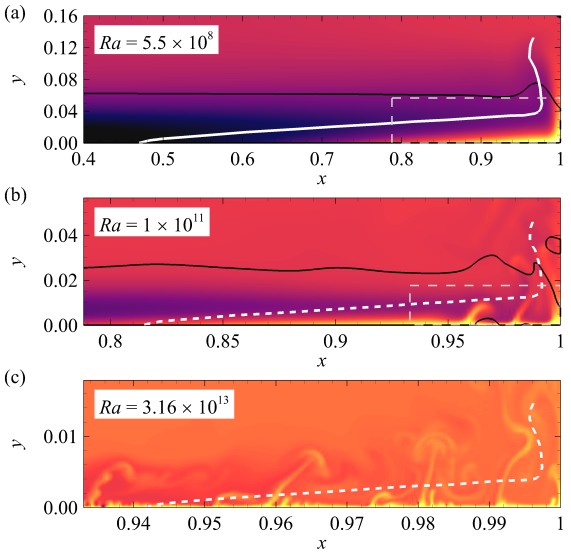

Figure 4: Detail view of the temperature fields at the hot end of the forcing boundary at Rayleigh numbers as shown. (a) shows the right-hand 60% and full height of the enclosure. (b) and (c) zoom in on the bottom-right-hand 35.3% and 11.2% of the frame coverage in (a), following the $Ra^{-1/5}$ scaling of the boundary layer and end-wall plume (Mullarney *et al.*, 2004; Sheard and King, 2011). The unbroken white line in (a) marks the perimeter of the thermal boundary layer and end-wall plume. The dashed lines in (b) and (c) shows where this perimeter would scale down to at the higher Rayleigh number following Rossby's $Ra^{-1/5}$ scaling. While each frame depicts a different Rayleigh number, the dashed rectangular boxes in (a) and (b) illustrate the respective plot areas shown in (b) and (c) to reinforce the smaller scales with increasing Ra. Dark to light contours respectively show cold ($\theta = \delta\theta/2$) to hot ($\theta = \delta\theta$) fluid, and the solid black line indicates zero horizontal velocity: below this line flow is left to right, above is right to left.

ported directly into the bulk overturning flow beyond the boundary layer. The individual plume eruptions entrain nearby fluid from within the boundary layer: this sweeping significantly increases the vertical thermal gradient along the base between the plumes, leading to the observed heat transport increase in this region.

Figure 4 compares the horizontal heat transport scenario satisfying Rossby's $Ra^{1/5}$ scaling argument in regime I/II (Figure 4a) with the elevated heat flux in the $Ra^{1/4}$ regime (Figure 4b,c), where the stable $Ra^{-1/5}$ thermal layer has been destroyed and replaced by plumes transporting heat vertically directly into the interior of the flow. Gayen *et al.* (2014) had suggested that a turbulent line plume model (Hughes and Griffiths, 2006) may explain their apparent recovery of a $Ra^{1/5}$ Nusselt number scaling at high Rayleigh number, but the conditions for such a model appear to be violated by the direct supply of heat to the interior bulk overturning flow captured here. It is possible that the large-eddy simulation modeling they employed for $Ra \gtrsim 5 \times 10^{10}$ may have been unable to resolve the delicate plume structures essential to this heat transport mechanism. Indeed, the plume filaments and thermal boundary layer in Figure 4(b,c) are at least an order of magnitude smaller than the former $Ra^{-1/5}$ thermal layer thickness at those Rayleigh numbers. The high-order low-dissipation scheme adopted in the present study is ideal for capturing these structures.

A $Nu \sim Ra^{1/4}$ scaling is well-known in natural convection: horizontal plates heated from below in mass flow experiments (Goldstein *et al.*, 1973) (where Sherwood number Sh is analogous to Nusselt number) correlate to $Nu = 0.59Ra^{1/4}$, and for inclined heated plates facing upward, (Fujii and Imura, 1972) obtained $Nu = 0.56Ra^{1/4}$. These are very close to the present regression $Nu = 0.59Ra^{1/4}$. Grossmann and Lohse (2000) construct a $1/4$ scaling (their regime I_u) from an argument that dissipation occurs primarily within the thermal and kinematic boundary layers at higher Prandtl numbers where the thermal boundary layer (thickness h_θ) is nested within the kinematic boundary layer (thickness h_u). The same scaling can also be obtained by modifying the plume scale analysis presented by Castaing *et al.* (1989): assuming that the conductive thermal boundary layer breaks into filaments of thickness similar to h_θ, which accelerate to the roll velocity u_c such that buoyancy balances the viscous force, then $\alpha g\,\delta\theta\,\rho_0 h_\theta \sim \mu u_c/h_u$. If u_c is proportional to the free-fall velocity (Xin *et al.*, 1996), one obtains $Nu \sim Ra^{1/4}Pr^{-1/12}$, an exact match to Grossmann and Lohse (2000).

Figure 3 demonstrates that horizontal convection heat transport strictly operates as a mixed regime (Grossmann and Lohse, 2000), with the stable forcing boundary layer obeying $Ra^{1/5}$ scaling while contributing only modestly to the overall heat transport, while the unstable plume region obeying the $Ra^{1/4}$ scaling at the hotter end contributes significantly to the overall heat transport. As the plumes elevate heat transport at the part of the base where heat transport was greatest under the $Ra^{1/5}$ scaling regime, the $Ra^{1/4}$ scaling dominates.

An alternative to the fixed-temperature forcing boundary considered here is a fixed-thermal-flux configuration (Mullarney *et al.*, 2004). We expect the same upward shift in scaling exponent to arise as both configurations manifest the same global flow behaviour, though some differences in the size or location of the $Ra^{1/4}$ plume region is inevitable due to the different temperature distribution along the forcing boundary under the flux-driven configuration.

The discovery of a $Ra^{1/4}$ regime in horizontal convection analogous to the I_u regime under the unifying theory of Grossmann and Lohse invites extrapolation to Rayleigh numbers beyond those achievable with contemporary compute capabilities. In Rayleigh–Bénard convection, the I_u regime is ultimately replaced by the IV_u regime beyond $Ra_{\mathrm{RBC}} \approx 10^{12}$, where the dominant contribution to thermal and molecular dissipation shifts from the boundary layers to the bulk interior. This regime scales as $Nu \sim Ra^{1/3}$, precisely the upper bound reasoned by Siggers *et al.* (2004). A $Ra^{1/3}$ scaling regime was captured at high Ra in early cooling wire experiments (Davis, 1922) and from a heated horizontal flat plate (Fujii and Imura, 1972). In the context of Rayleigh–Bénard convection in the limit of high Rayleigh number, heat flux reaches a finite limit independent of the enclosure height scaling with $Ra^{1/3}$ (Priestley, 1954), and (Malkus, 1954) recover a $Ra^{1/3}$ scaling from analysis of the turbulent regime in terms of the marginal stability of the mean flow.

We finally consider the oceanic implications of these results. Constructing a vertical Rayleigh number across the thermal boundary layer, $Ra_h = \alpha g \delta\theta h_\theta^3/\nu\kappa$, yields $Ra_h/Ra = (h_\theta/L)^3$. From (Mullarney *et al.*, 2004) we take $h_\theta/L = 2.649 Ra_F^{-1/6}$, $Nu = 0.81587 Ra_F^{1/6}$ and $Ra_F = NuRa$. Solving for Ra given the expected transition from the $1/4$ to the $1/3$ scaling regime at $Ra_h = 10^{12}$ yields $Ra = 1.4 \times 10^{37}$. Using representative values for Earth's oceans, Siggers *et al.* (2004) estimates an oceanic Rayleigh number $Ra = O(10^{31})$: this is 6 orders of magnitude below our estimated $Ra^{1/3}$ regime threshold, which suggests that the $1/3$ regime is unlikely to emerge in Earth's oceans. Hence with $Nu = 0.59 Ra^{1/4}$ expected to persist to oceanic scales, representative oceanic values (Siggers *et al.*, 2004) $\rho_0 = 10^3$ kg m^{-3}, specific heat capacity $c_p = 4200$ J kg^{-1} K^{-1}, $\kappa = 10^{-7}$ m^2 s^{-1}, $\delta\theta = 10$ K and $L = 10^7$ m yield a heat flux per unit area (Mullarney *et al.*, 2004) $F_T = \rho_0 c_p \kappa \delta\theta Nu/L = 24$ W m^{-2}. Taking a representative ocean surface area of approximately 2×10^{13} m^2 from the tropical Atlantic ocean yields a horizontal heat flux 4.7×10^{14} W. This is below the 2×10^{15} W estimate of equator-to-pole heat flux of planetary-scale ocean circulation (Munk and Wunsch, 1998), but is far closer than the 3.8×10^{12} W predicted from the $Ra^{1/5}$ scaling relation (from Figure 2). While these calculations are imprecise, not least due to questions around dissipation and Rayleigh number in real oceans (Mullarney *et al.*, 2004; Barkan *et al.*, 2013), and the choice of representative ocean area (e.g. dense water sinking near Greenland operates over an area of order 10^{12} m^2 whereas the total Atlantic ocean surface area is 1.06×10^{14} m^2), they nevertheless demonstrate the significance of the $1/4$ scaling regime towards the application of a horizontal convection model to Earth's oceans.

CONCLUSIONS

High-order spectral-element simulations identify a $Nu \sim Ra^{1/4}$ scaling regime in horizontal convection at high Rayleigh number, whose existence is explained by way of a vertical plume mechanism bypassing the horizontal convection transport mechanism in a manner consistent with natural convection from a heated horizontal flat plate. This reveals that the horizontal convection model plays a more important role than previously thought in explaining the ocean heat transport budget.

ACKNOWLEDGMENTS

This research has been supported by ARC Discovery Grants DP120100153 and DP150102920. Numerical simulations were performed using the high-performance computing resources of the National Computational Infrastructure (NCI) through the Merit Allocation Scheme. NCI is supported by the Australian Government.

REFERENCES

BARKAN, R. *et al.* (2013). "Rotating horizontal convection". *J. Fluid Mech.*, **723**, 556–586.

CASTAING, B. *et al.* (1989). "Scaling of hard thermal turbulence in Rayleigh–Bénard convection". *J. Fluid Mech.*, **204**, 1–30.

Chiu-Webster, S. *et al.* (2008). "Very viscous horizontal convection". *J. Fluid Mech.*, **611**, 395–426.

DAVIS, A.H. (1922). "Natural convective cooling in fluids". *Phil. Mag. S. 6*, **44(263)**, 920–940.

FUJII, T. and IMURA, H. (1972). "Natural-convection heat transfer from a plate with arbitrary inclination". *Int. J. Heat Mass Trans.*, **15(4)**, 755–767.

GAYEN, B. *et al.* (2014). "Stability transitions and

turbulence in horizontal convection". *J. Fluid Mech.*, **751**, 698–724.

GIANNAKOUROS, I.G. and KARNIADAKIS, G.E. (1994). "A spectral element-FCT method for the compressible Euler equations". *J. Comput. Phys.*, **115(1)**, 65–85.

GIRALDO, F.X. (1998). "The Lagrange–Galerkin spectral element method on unstructured quadrilateral grids". *J. Comput. Phys.*, **147(1)**, 114–146.

GOLDSTEIN, R.J. *et al.* (1973). "Natural convection mass transfer adjacent to horizontal plates". *Int. J. Heat Mass Trans.*, **16**, 1025–1035.

GROSSMANN, S. and LOHSE, D. (2000). "Scaling in thermal convection: A unifying theory". *J. Fluid Mech.*, **407**, 27–56.

GROSSMANN, S. and LOHSE, D. (2001). "Thermal convection for large Prandtl numbers". *Phys. Rev. Lett.*, **86(15)**, 3316–3319.

GROSSMANN, S. and LOHSE, D. (2002). "Prandtl and Rayleigh number dependence of the Reynolds number in turbulent thermal convection". *Phys. Rev. E*, **66(1)**, 016305.

HUANG, R.X. (1999). "Mixing and energetics of the oceanic thermohaline circulation". *J. Phys. Oceanogr.*, **29**, 727–746.

HUGHES, G.O. and GRIFFITHS, R.W. (2008). "Horizontal convection". *Annu. Rev. Fluid Mech.*, **40**, 185–208.

HUGHES, G.O. *et al.* (2007). "A theoretical model for horizontal convection at high Rayleigh number". *J. Fluid Mech.*, **581**, 251–276.

HUGHES, G. and GRIFFITHS, R. (2006). "A simple convective model of the global overturning circulation, including effects of entrainment into sinking regions". *Ocean Modelling*, **12(1)**, 46–79.

HUSSAM, W.K. *et al.* (2014). "The effect of rotation on radial horizontal convection and Nusselt number scaling in a cylindrical container". *Int. J. Heat Mass Trans.*, **77**, 46–59.

ILICAK, M. and VALLIS, G.K. (2012). "Simulations and scaling of horizontal convection". *Tellus A*, **64**, 18377.

KARNIADAKIS, G.E. and SHERWIN, S.J. (2005). *Spectral/*hp *Element Methods for Computational Fluid Dynamics*. 2nd ed. Oxford University Press, United Kingdom.

KARNIADAKIS, G.E. *et al.* (1991). "High-order splitting methods for the incompressible Navier–Stokes equations". *J. Comput. Phys.*, **97(2)**, 414–443.

MALKUS, W.V. (1954). "The heat transport and spectrum of thermal turbulence". *Proceedings of the Royal Society of London. Series A. Mathematical and Physical Sciences*, **225(1161)**, 196–212.

MULLARNEY, J.C. *et al.* (2004). "Convection driven by differential heating at a horizontal boundary". *J. Fluid Mech.*, **516**, 181–209.

MUNK, W. and WUNSCH, C. (1998). "Abyssal recipes II: Energetics of tidal and wind mixing". *Deep-Sea Res.*, **45**, 1977–2010.

PRIESTLEY, C.H.B. (1954). "Convection from a large horizontal surface". *Austral. J. Phys.*, **7**, 176–201.

ROSSBY, H.T. (1965). "On thermal convection driven by non-uniform heating from below: an experimental study". *Deep Sea Research and Oceanographic Abstracts*, vol. 12, 9–16. Elsevier.

SHEARD, G.J. and KING, M.P. (2011). "Horizontal convection: Effect of aspect ratio on Rayleigh number scaling and stability". *Appl. Math. Model.*, **35(4)**, 1647–1655.

SIGGERS, J. *et al.* (2004). "Bounds on horizontal convection". *Journal of Fluid Mechanics*, **517(1)**, 55–70.

STOMMEL, H. (1962). "On the smallness of sinking regions in the ocean". *Proc. Natl Acad. Sci.*, **48**, 766–772.

WUNSCH, C. and FERRARI, R. (2004). "Vertical mixing, energy, and the general circulation of the oceans". *Annu. Rev. Fluid Mech.*, **36**, 281–314.

XIN, Y.B. *et al.* (1996). "Measured velocity boundary layers in turbulent convection". *Phys. Rev. Lett.*, **77(7)**, 1266–1269.

